Electron dynamics of transition metal compounds studied with resonant soft x-ray scattering

J. Jiménez-Mier,[a] G. Herrera-Pérez,[a] P. Olalde-Velasco,[a,b] G. Carabalí,[a] E. Chavira,[c] P. de la Mora,[d]
W.L. Yang,[b] J. Denlinger,[b] A. Moewes,[e] and R. Wilks,[e].

[a]*Instituto de Ciencias Nucleares, Universidad Nacional Autónoma de México, México, D.F., 04510, México.*

[b]*The Advanced Light Source, Lawrence Berkeley National Laboratory, Berkeley, CA.*

[c]*Instituto de Investigaciones en Materiales, Universidad Nacional Autónoma de México, México D.F., 04510, México.*

[d]*Facultad de Ciencias, Universidad Nacional Autónoma de México, México D.F., 04510, México.*

[e]*Department of Physics and Engineering Physics, University of Saskatchewan, Canada.*

Recibido el 10 de marzo de 2010; aceptado el 31 de agosto de 2010

High resolution experimental data for resonant soft x-ray scattering of transition metal compounds are shown. The compounds studied are the ionic transition metal di-fluorides, ionic and covalent orthovanadates and members of the $La_{1-x}Sr_xCoO_3$ perovskite family. In all compounds we studied the transition metal $L_{2,3}$ edge and also the ligand (oxygen or fluorine) K edge. For the ionic compounds the transition metal data are in good agreement with atomic multiplet ligand field calculations that include charge transfer effects. Density functional calculations give very useful information to interpret the ligand x-ray emission data. The experimental metal L_α emission data show that the region between valence and conduction bands in the di-fluorides has several d-excited states. At the L_2 edge of the ionic orthovanadates we found the signature of a fast Coster-Kronig decay process that results in a very localized emission peak. Changes in the oxidation sate in the $La_{1-x}Sr_xCoO_3$ compounds are observed at both the metal $L_{2,3}$ edge and the oxygen K edge absorption spectra.

Keywords: Resonant inelastic x-ray scattering; transition metal oxides and fluorides; electronic structure; Coster-Kronig decay.

Se presentan datos experimentales para el esparcimiento resonante de rayos x en compuestos de metales de transición. Los compuestos estudiados son los difluoruros de metales de transición que son iónicos, ortovanadatos iónicos y covalentes, y varios miembros de la familia de Perovskitas $La_{1-x}Sr_xCoO_3$. En todos los compuestos estudiamos la orilla $L_{2,3}$ del metal de transición y la orilla K del ligando (oxígeno o flúor). Para los compuestos iónicos los datos del metal de transición están en buen acuerdo con cálculos de multiplete atómico con campo ligante que incluyen transferencia de carga. Cálculos que emplean funcionales de densidad dan información muy útil para interpretar los datos de emission de rayos x en la orilla del ligando. Los datos de emisión L_α muestran que la región entre las bandas de valencia y conducción en los difluoruros tiene estados excitados d. En la orilla L_2 de los ortovanadatos iónicos encontramos características de un proceso Coster-Kronig de decaimiento que da lugar a un pico de emisión muy localizado. En las orillas $L_{2,3}$ del metal y K de oxígeno se observaron cambios en el estado de oxidación en los compuestos $La_{1-x}Sr_xCoO_3$.

Descriptores: Esparcimiento inelástico de rayos x; óxidos y fluoruros de metales de transición; estructura electrónica; decaimiento Coster-Kronig.

PACS: 78.70.Ck; 78.70.En

1. Introduction

X-Ray spectroscopies are well established tools to study the electronic structure and dynamics of condensed matter systems [1, 2]. In X-Ray absorption an inner shell electron is promoted into unoccupied states of the continuum. It therefore probes the unoccupied density of states. X-Ray emission is the complementary process in which a valence electron makes a transition to fill an inner shell hole. In this case one obtains information about the occupied density of states. There are several advantages to the use of x-rays to study condensed matter systems. To begin with, the absorption edge and the emission lines are element sensitive. In the soft x-ray regime both kind of transitions follow the electric dipole selection rules. Thus, with x-ray spectroscopies one gets detailed information about density of states localized at specific atoms and with well defined values of the orbital angular momentum. Also, the incoming and outgoing x-rays have a relatively long penetrating depth, and one thus obtains information about the sample bulk.

In resonant inelastic x-ray scattering (RIXS) one uses the excitation produced by an incoming x-ray photon and then studies the x-ray emission that follows the resonant creation of an inner shell hole. In the RIXS process the charge state of the ion that is being probed does not change. This is another advantage compared to independent x-ray absorption and normal emission spectroscopies. Also, by measuring the resonant emission spectrum as a function of the difference in energy between the incoming and outgoing electron (the energy loss) one obtains information about excited states of the ground configuration that are usually dipole-forbidden for direct optical excitations.

The transition metals form compounds with a wide arrange of properties and many direct applications. The $L_{2,3}$ absorption edge of all the $3d$ transition metals is in the soft x-ray energy region, between 400 and 100 eV. Their compounds are excellent candidates to be studied at soft x-ray fluorescence beamlines of synchrotron radiation sources. In this paper we present three examples of the kind of information that can be obtained by using absorption and resonant emission x-ray spectroscopies of transition metal compounds. In the first one we study the family of the most ionic transition compounds, namely, the di-fluorides. One can also study the behavior of the fluorine K-edge. In the second example we study the excitation and decay dynamics of vanadium oxides. Again, x-ray absorption and resonant emission spectra were taken at both the vanadium $L_{2,3}$ and oxygen K edges. Finally, in the last example we use oxygen and cobalt soft x-ray spectroscopies to study the effect of strontium doping in the $La_{1-x}Sr_xCoO_4$ perovskite family.

2. Experiment

The experiments took place at beam line 8.0.1 of The Advanced Light Source in Berkeley. Details of the beam line can be found elsewhere [3]. The radiation is produced in a 5.0 period undulator. It is monochromatized by one of three gold-coated spherical gratings and then it is focused onto the sample. The x-ray absorption signal is monitored by the total sample current. This results in total electron yield (TEY) spectra.

At selected values of the excitation energy of each TEY spectra we also record x-ray emission spectra. For the difluorides or the cobalt perovskites this was done at a low-background soft x-ray spectrometer [3]. It detects photons emitted at right angles with respect to the incoming beam, along its polarization direction. It has four different gratings that cover the photon energy range between 100 and at least $1000\ eV$. A variable entrance slit allows control over the spectrometer resolution. The emission spectra are recorded with a position sensitive detector mounted along the Rowland circle. The spectrometer photon energy at the $L_{2,3}$ edge of the metals was calibrated using the elastic emission. To calibrate emission at the fluorine K-edge we used the values reported by Esmail and Urch [5]. The O-K emission energy was calibrated with the normal ZnO spectra recorded at second order.

The emission spectra of the orthovanadates were obtained in a soft x-ray spectrometer that is based on an entrance slitless design, a spherical collecting mirror, a variable line spacing grating, and a charge coupled device detector (CCD) [4].

The fluorides and the V_2O_5 sample were all commercial powders of purity greater than 98%. The YVO_4 was a polycrystalline sample prepared by sol-gel reaction [6]. We also prepared, but by solid state reaction, powder samples of three members of the Perovskite family $La_{1-x}Sr_xCoO_3$ with $x = 0$, 0.3, and 0.5 [7].

3. Theory

Resonant x-ray scattering is a coherent second order process that is described by the Kramers-Heisenberg expression:

$$\sigma(\nu_1,\nu_2) \propto \sum_f |\sum_i \frac{<f|\vec{e}_2\cdot\vec{r}|i><i|\vec{e}_1\cdot\vec{r}|g>}{h\nu_1-(E_i-E_g)-i\Gamma_i/2}|^2 \times \delta[h(\nu_1-\nu_2)-(E_f-E_g)] \quad (1)$$

where $|g>$, $|i>$ and $|f>$ are the initial-, intermediate-, and final-state wavefunctions with energies E_g, E_i, and E_f respectively. The transition operator $\vec{e}\cdot\vec{r}$ assumes that all are electric dipole transitions, and the delta function assures overall conservation of energy.

In this paper we make the calculation for the metal resonant emission using the atomic-multiplet ligand field codes [2] that may also include charge transfer. The wavefunctions and transition matrix elements are taken from a single-configuration Hartree-Fock calculation [8]. The ligand field parameters $10D_q$, D_s and D_t [2] are then varied until the best agreement between experiment and theory for the x-ray absorption spectra is found. The transition energies and transition matrix amplitudes are then directly substituted into the Kramers-Heisenberg formula (Eq. 1) to obtain emission spectra.

The fluorine absorption and emission spectra are compared with $2p$-projected density of states. The calculations were done with the WIEN2k package [9], which is an all-electron full-potential linearized augmented plane wave (FP-LAPW) method based on density functional theory (DFT). The strong correlations on the transition metals were included via $LDA+U_H$ (SIC) using the method proposed by Madsen and Novák [10]. The generalized gradient approximation (GGA) of Perdew, Burke and Ernzerhof [11] was used for the treatment of the exchange-correlation interactions. The energy threshold to separate localized and non-localized electronic states was 6 Ry. The muffin-tin radii (MT) were chosen in such a way that no more than $0.01e$ leak out of the muffin tin sphere. The criterion for the number of plane waves was $R^{MT}_{min}\times K^{max}=9$ and the number of k-points was $9\times9\times12$ for CrF_2 and MnF_2, $8\times8\times12$ for FeF_2 CoF_2 and CuF_2, and $8\times8\times13$ for NiF_2 and ZnF_2.

4. Results and discussion

We now present examples of the information about electronic estructure and dynamics of transition metal compounds that can be obtained with soft x-ray absoption and emission spectroscopies.

4.1. Transition metal difluorides

We start the discussion with the family of the most ionic transition metal compounds, namely, the transition metal difluorides MF_2 with M=$Cr-Zn$. Here we have added Zn to

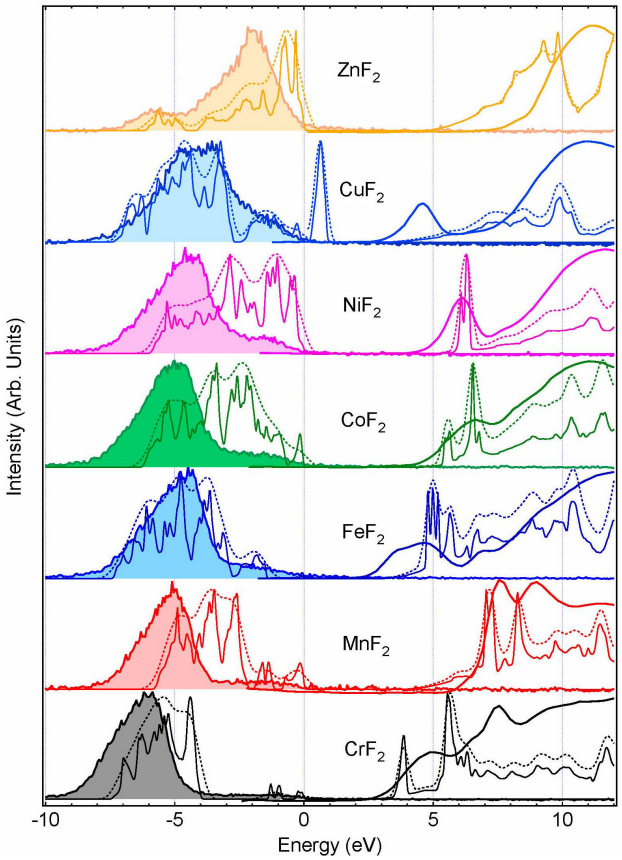

FIGURE 1. Absorption and emission spectra of the MF_2 (M=$Cr-Zn$) difluorides at the fluorine K-edge. We also show the calculated fluorine 2p density of states (DOS) for the valence and conduction bands. In all plots the thick solid line gives the experimental data. The emission spectra are also shaded. The solid thin lines are the calculated DOS and the dashed lines are the result of the convolution with the instrument window functions. For details see the text.

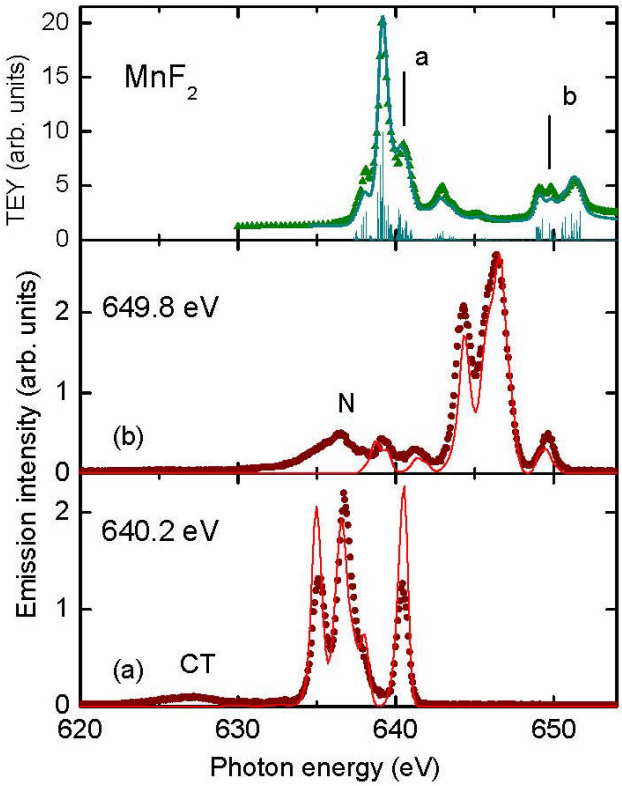

FIGURE 2. Comparison between the absorption and emission spectra of MnF_2 at the manganese $L_{2,3}$-edge and the results of an atomic-multiplet ligand field calculation. Top panel: comparison for absorption. The experimental data are the solid green triangles, the calculation are the cyan lines. Bottom panels: emission spectra recorded at the excitation energies a and b. The experimental data are the solid bullets, the red continuous line is the calculated spectra. It cannot reproduce the charge transfer (CT) nor the normal emission (N) peaks (see text).

cover the whole $3d^n$ series up to the completely filled 3d shell.The crystal structure of the whole family is simple enough (rutile or distortd rutile) to allow relatively straightforward density functional calculations. On the experimental side, all of the metal $L_{2,3}$ absorption edges and the fluorine K edge fall in the sot x-ray region between 550 and 1100 eV.

In Fig. 1 we make a comparison between experiment and the calculated fluorine $2p$ projected density of states (pDOS) for absorption and normal emission in the whole series. We take the total electron yield (TEY) spectra as representative of x-ray absorption, and the emission recorded with an excitation energy of 700 eV for normal emission spectra. The calculated pDOS curves were constructed by taking the average of spin up and spin down densities of our antiferromagnetic calculation. We also show the convolution of the theoretical curves with triangular functions whose widths (FWHM) are 0.36 eV and 0.70 eV to take into account, respectively, the resolution of the monochromator for absorption and the combined resolution of the spectrometer and the monochromator for emission. The absorption and emission energy scale was determined so that the zero corresponds to the top of the valence band. A detailed discussion of the fluorine K-edge behavior of these compounds is presented elsewhere [12].

There is, in general, very good agreement between experiment and theory. The behavior of the band gap is well reproduced by theory. It increases in going from Cr to Mn, then decreases for Fe with a gradual increase in the series up to Ni. For CuF_2 theory predicts a sharp, low lying peak very close to the Fermi edge. Experiment confirms this, but the peak appears about 4 eV higher. The metal $3d$ orbitals play a very important role, through hybridization, in the structure of the conduction band. All absorption spectra in the series up to CoF_2 have two sharp peaks riding on broader features whose shape remains pretty constant throughout the entire series. The position and relative intensity of the sharp peaks is different for each compound. In NiF_2 and CuF_2 there is only a sharp peak that corresponds, in a simple molecular orbital picture, to a single empty e_g metal orbital. The sharp metal $3d$ peaks are completely absent in the absorption structure of ZnF_2.

The emission spectra of all members of the series has the same overall structure. It has a large peak with a low energy

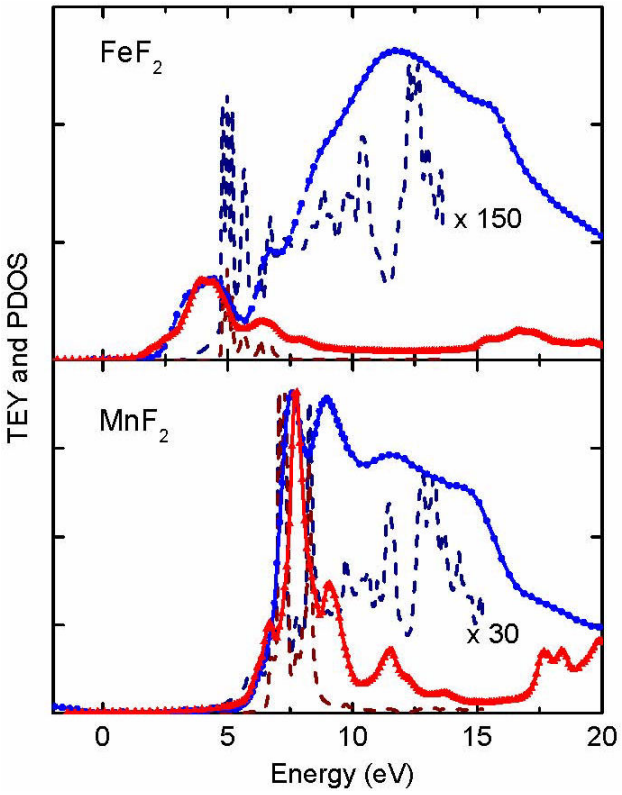

FIGURE 3. Comparison between the fluorine K and metal L_3 absorption edges in MnF_2 and FeF_2. The dashed lines are the results of the DOS calculation. Blue solid bullets: experimental fluorine K absorption; red solid triangles: experimental metal $L_{2,3}$ absorption. Dark blue dashed line: calculated F $2p$ DOS; dark red dashed line: calculated metal $3d$ DOS.

tail and a rather broad high energy satellite that extends to the top of the valence band. However, there are significant differences among the compounds. The intensity of the satellite increases and its width decreases as we go from Cr to Cu (bottom to top). For ZnF_2 the satellite appears on the low energy side. Again, there is good overall agreement between experiment an theory for the whole series. The agreement is best for chromium, iron, copper and zinc. For manganese, cobalt and nickel the calculation gives a broader fluorine 2p band compared to the observed one.

Important, complementary information about these compounds can be obtained by looking at the resonant inelastic x-ray scattering spectra obtained at the transition metal $L_{2,3}$ absorption edge. In Fig. 2 we present the total electron yield (absorption) and two resonant emission spectra of MnF_2. The absorption spectrum is identical to the one reported previously [13, 14], while the emission spectra shown here were taken with a factor of four better resolution [13]. We also show the absorption and emission results of an atomic-multiplet, ligand field calculation. The absorption spectrum was obtained using the codes developed by de Groot [2]. They start with a free ion calculation of the multiplet structure that is then split by a D_{4h} ligand field. No charge transfer effects were included in this analysis. Theory then gives a series of transitions indicated by the vertical lines in the top spectrum. Broadening effects are taken into account by convolution of the absorption lines with Lorentzian (lifetime) and Gaussian (instrument) functions.

There is very good agreement between experiment and theory, indicating that the main ingredients of the absorption spectra were included in the calculation. The other two plots in Fig. 2 make a comparison between the experimental and theoretical emission spectra excited with the energies marked a and b in the TEY spectrum. The experimental data were corrected for self absorption [15]. The theoretical results were obtained by substituting the same parameters (multiplet structure and ligand field $10D_q$, D_s and D_t) of the absorption calculation into the Kramers-Heisenberg expression, Eq. 1. These data were further broadened with a Gaussian window to include the finite spectrometer resolution. Once again, there is very good agreement between experiment and theory, with the main discrepancy coming from different relative intensities of the main emission peaks. The calculation does not predict the broad, low energy emission (CT and N) peaks. The first one (CT) originates from the hybridization between the manganese $3d$ and the fluorine $2p$ orbitals. The second one (N) is the normal emission peak that results from the decay of the non-resonant production of a $2p_{3/2}$ hole. The multiplet portion of emission that is very well reproduced by the calculation has the same overall structure in both spectra. It has a high energy sharp elastic peak followed by emission peaks that results from transitions leaving the manganese ion in d-excited states [13]. In the case of excitation at the L_2 edge (b in Fig. 2) there are two features around 640 eV that indicate production of $S = 1/2$ d-excited states [13].

Now we know that a band DOS calculation allows a direct interpretation of the fluorine K absorption spectra while an atomic calculation reproduces very well the multiplet structure of the metal $L_{2,3}$ absorption edge. Thus, it is interesting to directly compare the fluorine and metal absorption spectra. The comparison for MnF_2 and FeF_2 is made in Fig. 3. The energy scale for fluorine K absorption is taken directly from Fig. 1. We shifted down the metal $L_{2,3}$ edge and adjusted its intensity to achieve the best overlap with the corresponding sharp features at the fluorine K-edge. For comparison in the figure we also show the calculated DOS for both fluorine and the metal. It is clear that in the two compounds the sharp peaks are due to hybridization with the metal $3d$ DOS. Also, this hybridization is only important within a few eV of the beginning of the absorption edge. Theory also predicts that the broad absorption structure above these sharp features is due to hybridization that does not contain metal $3d$ orbitals. What is surprising in Fig. 3 is that some of the details of the metal absorption are also present at the fluorine K-edge. For instance, the two small peaks in iron around 7.5 eV correspond to two shoulders in the fluorine absorption spectrum. Therefore one can conclude that there is evidence of the atomic multiplet structure in the fluorine absorption edge.

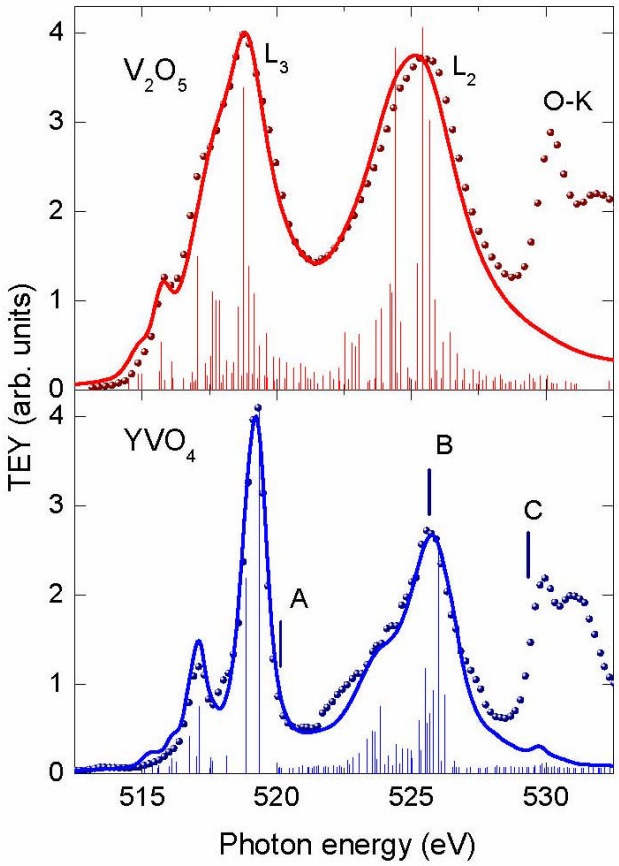

FIGURE 4. Comparison between the soft x-ray absorption spectra of V_2O_5 and YVO_4 and the result of atomic multiplet calculations that include ligand field and charge transfer effects. Top panel V_2O_5: the red bullets are the experimental data, the thin red vertical lines are the calculated transitions and the thick red line is the result of broadening the transitions. Bottom panel YVO_4: the blue bullets are the experimental data, the thin blue vertical lines are the calculated transitions and the thick blue line is the result of broadening the transitions.

4.2. Electron dynamics of vanadium oxides

Near the low end of the transition metal row, vanadium can form compounds with a $5+$ oxidation state. These orthovanadates are an ideal test ground to study the electron dynamics of a $3d^0$ transition metal compound. Here we present results of a comparison between two $3d^0$ vanadium compounds, namely V_2O_5 and YVO_4. In Fig. 4 we show the x-ray absorption spectra of these compounds. The vanadium $L_{2,3}$ edges are the first ones to appear, immediately followed by the oxygen K-edge. The $L_{2,3}$ spectra of both compounds are compared with the results of atomic multiplet calculations. They include ligand field and charge transfer effects. As a result of charge transfer the ground state is an admixture of the $3d^0$ and $3d^1\underline{L}$ configurations, where $\underline{L}$ represents a ligand hole. For V_2O_5 the mixing coefficients are 50 - 50, which is a sign of strong hybridization. For YVO_4 the mixing is 72 - 28, indicating a more ionic compound. This configuration mixing was crucial to achieve such a good agreement between experiment in V_2O_5. In YVO_4 it was more important to adjust the lifetime broadening in different regions of the spectrum. For the low energy peak (at about 516 eV) we directly took the metal width $\Gamma_{2p} = 0.23$ eV [16]. For the maximum of L_3 (at about 518 eV) theory predicts two major transitions that will play an important role later on. They had to be broadened by 0.48 eV, more than twice the $2p$ hole width. The lifetime broadening in the L_2 region is much larger, 1.4 eV. This gives the first piece of information about the fast Coster-Kronig decay of the $2p_{1/2}$ core hole.

Now we present examples of emission spectra for the ionic YVO_4 compound. They are shown in Fig. 5. In the bottom panel we make a comparison between two almost resonant spectra, one recorded for an excitation energy just after the L_3 absorption peak in vanadium (A), and the other just

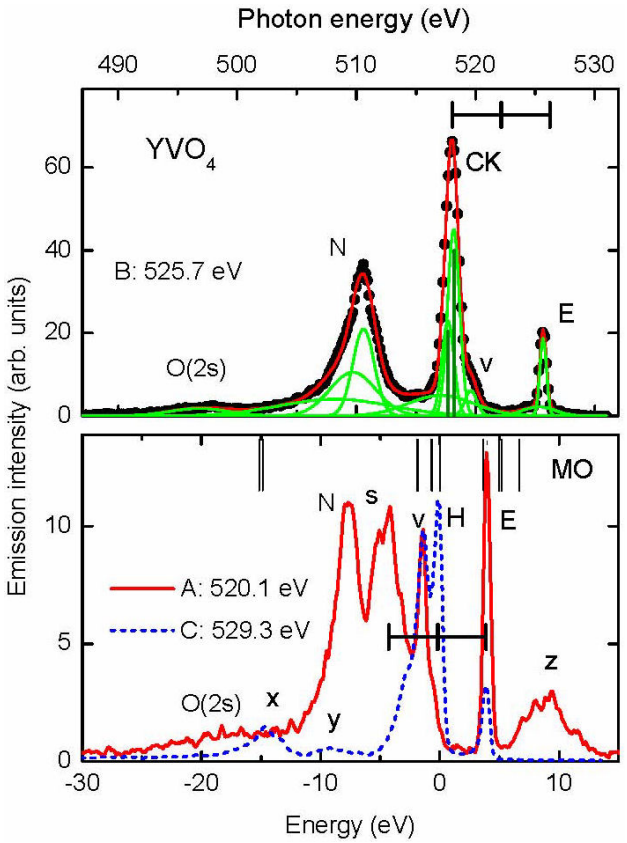

FIGURE 5. Soft x-ray emission spectra of YVO_4. Bottom panel: comparison between the emission spectra obtained just after the L_3 maximum (A: solid red line) and just before the O-K maximum (C: dashed blue line). The spectra were shifted so that the elastic emission at both energies coincided and the zero was chosen at the top of the emission peak H. The vertical bars give the energy position of the states in a molecular orbital calculation [17]. For the rest of the labels see text. Top panel: emission spectrum for an excitation energy at the maximum of the L_2 absorption spectrum (B). The bullets are the experimental data, the green lines are the ten Gaussians fitted and the red line is their sum. We indicate with two vertical lines the centers and relative intensities of the two transitions under the Coster-Kronig peak. See text.

before the oxygen K maximum (C). The energy scale was shifted to make the elastic peaks of both spectra coincide, and at the same time put zero energy at the maximum of the oxygen K emission (peak H). In this panel we also include the positions of molecular orbitals calculated for this compound [17]. The vanadium emission spectrum (A) has a high energy oxygen peak (z) that results from excitation with higher orders of the undulator radiation. Then there is a strong, sharp elastic peak (E) followed by valence emission (v), a satellite (s) that results from the simultaneous excitation of two valence electrons, the normal emission peak (N) and a broad emission feature at the energy of the oxygen $2s$ orbitals. The oxygen spectrum (C) begins with a smaller elastic peak (E) followed by a sharp peak (H) that corresponds to emission from the highest occupied molecular orbital (HOMO), a second valence peak (v) and peaks x and y that result from normal vanadium emission. It is really remarkable that aligning the elastic peaks (E) of both spectra also results in aligned valence emission peaks (v), and the comparison with the molecular orbital calculation is also direct. In the vanadium spectrum (A) the valence peak (v) and and a small high energy shoulder correspond to the two occupied molecular orbitals just before the HOMO. In the oxygen spectrum (C) peak H can be identified with the HOMO and the elastic is not too far from the calculated LUMO. The lowest MO's in the plot correspond to the oxygen $2s$ broad peak. This assignment is also in agreement with the MO calculation that gives a dominant oxygen character to the HOMO [17]. The difference in energy between (E) and (H) is a direct measure of the bandgap, which in this case is equal to 3.9 eV. Now, satellite (s) is centered at twice the bandgap (marked by the bars in the spectrum) from the elastic peak , indicating a double electron excitation. The peaks analyzed thus far, together with the O(2s) broad stucture, result from the resonant inelastic scattering process described by the Kramers-Heisenberg expression (Eq. 1). The normal (N) emission peak is the only one that does not move when the excitation energy is changed, and results because of the non-resonant production of a $2p_{3/3}$ hole.

The top spectrum in Fig. 5 allows us to study the Coster-Kronig decay of the $2p_{1/2}$ hole. This is a non-radiative process in which the $2p_{1/2}$ hole produced resonantly at L_2 (B in Fig. 4) is transfered to the $2p_{3/2}$ subshell with the excess energy taken by a valence electron that jumps into the conduction band. For this low Z transition metal the CK decay strongly depends on the detailed electronic structure of the valence and conduction bands [18]. We performed a ten Gaussian fit routine to describe the top spectrum in Fig. 5. Sharp peaks were used for the elastic (E) and the Coster-Kronig (CK) peaks, while broad peaks were used for the oxygen $2s$, normal (N), a background peak under the CK, and the residual oxygen K emission that is under the elastic peak. Except for the CK peaks, the center, width and intensity of all other gaussians were free parameters in the fit. If one compares this emission spectrum with the absorption spectrum of Fig. 4 one can conclude that the CK peak corresponds to the peak at the L_3 maximum. The calculation puts two transition lines under this peak, separated by 0.48 eV and with an intensity ratio close to $2:1$. In the fit procedure for the CK peaks we used two lines separated by this energy, with the same intensity ratio and with *equal widths*. The two vertical bars give the fitted transitions. As in the lower panel, the black bars on top of the top spectrum give the energy needed for a double electron excitation. This is precisely the energy difference between the elastic and the top of the CK peak. The fact that the CK retains its shape (two transitions with the same separation and intensity ratio as in L_3) and is the dominant emission peak clearly indicate that the $3d$ excited electron remains a spectator during the CK decay. The width of the two CK lines that results from the fit is 1.18 eV. This is too large even when one considers the combined effect of the monochromator and spectrometer, which result in the 0.61 eV of the elastic peak. Thus, there is an extra broadening of the lines due to a fast decay process. If one subtracts in quadrature this instrument width, which is the combined effect of both monochromator and spectrometer, the result is a $2p$ hole width of 1.02 eV. Using Heisenberg uncertainty principle [16] one ends up with a $2p$ hole decay lifetime of 644 attoseconds.

4.3. The $La_{1-x}Sr_xCoO_4$ Perovskite family

Here we present the last example of the use of x-ray absorption and emission to study the electronic structure of some members of the $La_{1-x}Sr_xCoO_4$ perovskite family. The parent compound ($x = 0$) is a semiconductor [19] below room temperature. The cobalt appears as Co^{3+}. The ground, nonmagnetic state is obtained from the low-spin configuration t_{2g}^6. For high temperatures there is a change into higher spin configurations [19]. The strontium doping has the effect of oxidizing the cobalt, thus changing its valence to Co^{4+}.

In Fig. 6 we present a comparison between the absorption and normal emission spectra of the three members of the family. The samples were all at room temperature. The $x = 0$ absorption spectrum is in good agreement with previous results [20, 21]. There are noticeable changes in both absorption and emission as the amount of strontium in the compound is changed. The L_3 edge for $X = 0$ has a small, low energy shoulder, followed by the maximum absorption peak and a high energy shoulder. For $X = 0.3$ and 0.5 the absorption spectra are almost identical. They both show a larger low energy shoulder. The main absorption peak is not as sharp as that for $x = 0$, and the high energy peak is almost completely absent. The emission spectra are dominated by two features. The low energy one, labeled p, corresponds to emission from the valence band in the ground state. The higher energy, sharp peak (d) occurs because of emission from d-excited states of the valence band. This d peak is more intense and appears much closer to the L_3 maximum for $x = 0$. For $x = 0.3$ and 0.5 peak p moves to lower energies and peak d has lower intensity. Calculations are underway to study atomic multiplet effects in these spectra. It will also be very important to make

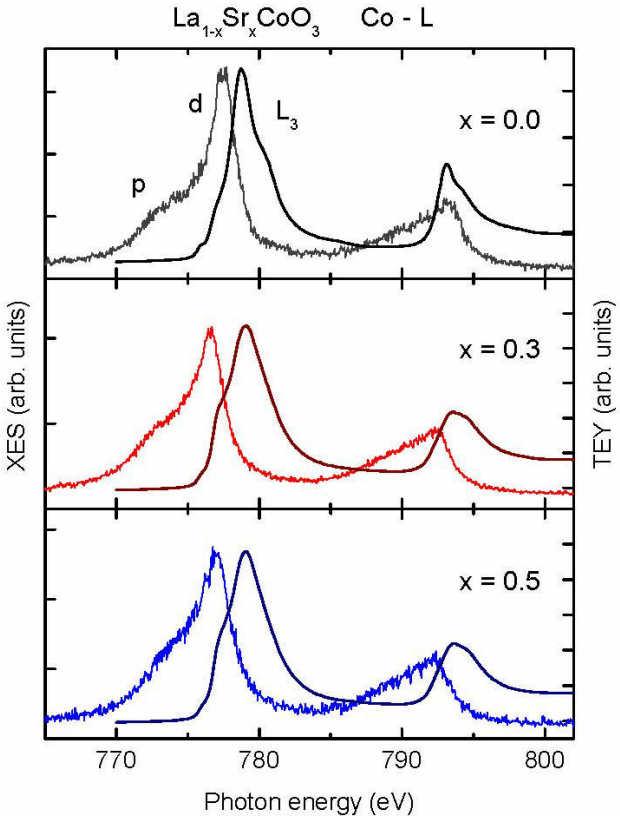

FIGURE 6. Cobalt x-ray absorption (right) and normal emission (left) spectra of the $La_{1-x}Sr_xCoO_4$ compounds.

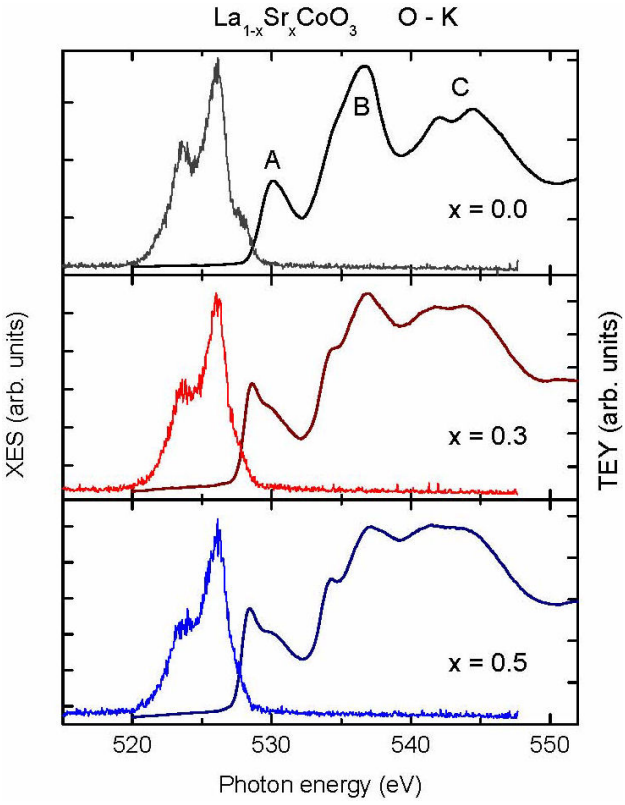

FIGURE 7. Oxygen x-ray absorption (right) and normal emission (left) spectra of the $La_{1-x}Sr_xCoO_4$ compounds.

a study of temperature effects in the absorption and emission of this perovskite family.

A similar comparison can be made at the oxygen K edge. The room temperature results are shown in Fig. 7. Here we compare the oxygen k absorption and emission spectra for $x = 0$, 0.3 and 0.5. Once again, there are important differences for different values of x. The absorption spectra are in good agreement with those reported by Toulemonde *et al.* [19]. They are divided into three different regions. Peak A results from excitation of an oxygen $1s$ electron into states that result from hybridization between oxygen $2p$ and cobalt $3d$ orbitals [19]. The features in the broad region B correspond to excitation into bands that are hybridizations of La($5d$)/Sr($4s$) and O($2p$) orbitals [19]. Finally, region C appears because of transitions into bands that result from the hybridization of cobalt $4sp$ and oxygen $2p$ states [19]. The changes introduced by the strontium doping are very clear in the absorption data. In region A a sharp peak to the low energy side appears, and a shoulder to the high energy side gets broader and more intense as x changes from 0.3 to 0.5. The low energy shoulder of feature B becomes sharper as x increases. Finally, the doublet structure of feature C smears out with increased strontium doping. There are also significant changes with x in the oxygen emission spectra. The general shape is the same, with two sharp peaks and a high energy shoulder that gives the position of the Fermi energy. The relative intensities of these three features change with x. The high energy shoulder is better defined for $x = 0$ and is almost completely gone at the higher doping ratios. Once again, density functional calculations are underway to try to explain this behavior.

5. Conclusions

We have presented experimental data for soft x-ray absorption and emission of several transition metal compounds. Theory was an important guide to interpret the results. The data for the transition metal di-fluoride series at the fluorine K edge was in good agreement with band like calculations for the fluorine p-projected density of states. A more localized model, the atomic multiplet with ligand field calculation, gave good results for both absorption and resonant emission at the transition metal $L_{2,3}$ edge. We found the signature of the metal multiplet structure in the fluorine F - K absorption. By adding charge transfer effects to an atomic multiplet calculation we were able to explain the $L_{2,3}$ absorption edge of vanadium oxides. In this case the metal and oxygen RIXS spectra were in direct correspondence with calculated molecular orbital states. They also contained information about two-electron excitation processes in the metal. We studied the fast Coster-Kronig decay of the $2p_{1/2}$ hole produced resonantly. We were able to study the effect of replacing lanthanum with strontium ions in the $La_{1-x}Sr_xCoO_3$ perovskites. We found changes in the oxygen and cobalt absorption and emission spectra as the strontium doping was

varied. More experiments and calculations are underway to further study these cobalt compounds.

Acknowledgments

This work was performed at the Advanced Light Source, which is supported by DOE (DE-AC03-76sF00098). This work was partly supported by CONACyT under project No. 56764. P. Olalde-Velasco would like to thank the *Beca Mixta* program of CONACyT, Mexico.

1. A. Kotani and S. Shin, *Rev. Mod. Phys.* **73** (2001) 203.
2. F.M.F. de Groot and A. Kotani, *Core Level Spectroscopy of Solids* (CRC Press, Boca Raton, Florida, 2008).
3. J.J. Jia *et al.*, *Rev. Sci. Instrum.* **66** (1995) 1394.
4. O. Fuchs *et al.*, *Rev. Sci. Instrum.* **80** (2009) 063103.
5. E.I. Esmail and D.S. Urch, *Spectrochimica Acta* **39A** (1983) 573.
6. G. Herrera *et al.*, *J. Sol-Gel Sci. Technol.* **46** (2008) 1.
7. J. Jiménez-Mier, G. Caravalí, P. Olalde-Velasco, E. Chavira, W.L. Yang, J. Denlinger, unpublished results.
8. R.D. Cowan, *The Theory of Atomic Structure and Spectra* (University of California Press, Berkeley, 1981).
9. Blaha, K. Schwarz, G.K H. Madsen, D. Kvasnicka, and J. Luitz, *WIEN2K: An Augmented Plane Wave and Local Orbitals Program for Calculating Crystal Properties* (Vienna University of Technology, Austria, 2001).
10. G.K. Madsen and P. Novák, *Europhys. Lett.* **69** (2005) 777; www.wien2k.at/reg user/textbooks/Constraint U.pdf
11. J.P. Perdew, K. Burke and M. Ernzerhof, *Phys. Rev. Lett.* **77** (1996) 3865.
12. P. Olalde-Velasco, W.L. Yang, J. Denlinger , P. de la Mora, and J. Jiménez-Mier, unpublished results.
13. J. Jiménez-Mier, D.L. Ederer and T.A. Schuler, *Phys. Rev. A* **72** (2005) 052502.
14. J. Jiménez-Mier *et al.*, *Rev. Mex. Fís. S* **53** (2007) 38.
15. J. Jiménez-Mier *et al.*, *Phys. Rev. B* **65** (2002) 184105.
16. M.O Krause and J.H. Oliver, *J. Phys. Chem. Ref. Data* **8** (1979) 329.
17. V.A. Gubanov, D.E. Ellis, and A.A. Fotiev, *J. Sol. State Chem.* **21** (1977) 303.
18. P. Le Fèvre *et al.*, *Phys. Rev. B* **69** (2004) 155421.
19. O. Toulemonde, N. N'Guyen, F. Studer, and A. Traverse, *J. Sol. State Chem.* **158**, (2001) 208.
20. M. Abbate *et al.*, *Phys. Rev. B* **47** (1993) 16124.
21. M. Magnuson, S.M. Butorin, C. Såthe, J. Nordgren, and P. Ravindran, *Europhys. Lett.* **68** (2004) 289.